Physical Chemistry Chemical Physics

PCCP

Gene transfer on inorganic/organic hybrid silica nanosheets

Journal:	*Physical Chemistry Chemical Physics*
Manuscript ID:	CP-ART-06-2015-003483.R1
Article Type:	Paper
Date Submitted by the Author:	13-Aug-2015

Complete List of Authors:	Huang, Nien-Chi; National Taiwan University, Polymer Science and Engineering Ji, Qingmin; National Institute for Materials Science, World Premier International (WPI) Research Center for Materials Nanoarchitectonics (MANA) Yamazaki, Tomohiko; National Institute for Materials Science, Biomaterials Center Nakanishi, Waka; National Institute for Materials Science, Hanagata, Nobutaka; National Institute for Materials Science, Nanotechnology Innovation Center Ariga, Katsuhiko; National Institute for Materials Science, World Premier International (WPI) Research Center for Materials Nanoarchitectonics (MANA) Hsu, Shan-hui; National Taiwan University,

Physical Chemistry Chemical Physics

ARTICLE

Gene transfer on inorganic/organic hybrid silica nanosheets

Received 00th January 20xx,
Accepted 00th January 20xx

DOI: 10.1039/x0xx00000x

www.rsc.org/

Nien-Chi Huang[a], Qingmin Ji[b], Tomohiko Yamazaki[b], Waka Nakanishi[b], Nobutaka Hanagata[b], Katsuhiko Ariga[b,c,*], Shan-hui Hsu[a,d,*]

Gene delivery is often accomplished by the forward or reverse transfection protocol. In either protocol, a transfection reagent (usually cationic) is added to increase the delivery efficiency. In this study, we employed a series of nanosheet networks to facilitate the delivery of naked plasmid DNA into human mesenchymal stem cells (hMSCs). By putting different chemicals into the reaction mixture for etching the silica glass, we were able to fabricate inorganic/organic hybrid nanosheet networks with different physico-chemical characteristics. We then analyzed the transfection efficiency on different nanosheets and the possible dependence of transfection efficiency on the physico-chemical parameters of nanosheets. Results showed that all nanosheet networks were noncytotoxic and demonstrated high cell survival rate (~90%) after transfection. The transfection efficiency was critically determined by the aspect ratio of the nanosheets (height/thickness of the wall). The effects from chemistry or other surface properties were not significant. Moreover, the transfection efficiency may be successfully predicted by the initial cell migration rate and activation of integrin β3 on the nanosheets. Compared to the conventional method, the transfection using concurrent cell/plasmid seeding on the nanosheets is not only more effective but also much safer. Future efforts may focus on combining the inorganic/organic hybrid nanosheets with soft substrates for in situ transfection.

1. Introduction

Transfection is a technique that delivers plasmid DNA or siRNA into cells to recombine DNA and to induce cell transformation[1]. Transfection can be achieved through chemical methods such as forming DNA complex with chemical reagents (e.g. cyclodextrin, liposomes, nanoparticles, and cationic polymers[2,3]) or physical methods such as electroporation, impalefection, magnet assisted transfection, and particle bombardment[4-7]. Although both methods can promote the intracellular delivery but they also cause inevitable cell death. The most common procedures of transfection was cell plating before adding the complex of transfection reagents and plasmid DNA, i.e. forward transfection[8]. Approaches to increase the forward gene delivery is focused on surface modification of nanoparticle carriers with aminoalkylsilanes and peptide for adjusting the size, zeta potential, and surface chemistry[9,10]. In addition, the studies have been demonstrated that the possibility of changing the cell culture substrate to increase the efficiency of gene delivery[11].

In contrast to forward transfection, the complex of transfection reagents and plasmid DNA in reverse transfection is adsorbed on certain culture substrates before cell seeding though this procedure is less frequently used[12,13]. The use of traditional transfection reagents was essential for either forward or reverse transfection. However, it is not as appropriate for transfection of stem cells because of the cytotoxicity[12,14]. Furthermore, the transfection efficiency of stem cells was obviously lower than that of cell lines[15,17]. Substrates for cell culture may be designed to have micro- or nanopatterns to increase the adsorption of the transfection reagent/DNA complexes to enhance the delivery of the plasmid into cells[14]. Substrate surfaces engineered with nanosheets[15], nanowires[16], or microchannels[17] were also reported to increase the transfection efficiency of plasmid complexes by reverse transfection. These studies demonstrate the possibility of modulating endocytosis rate by substrate topography. However, it remains very difficult to deliver naked plasmid DNA without

[a] *Institute of Polymer Science and Engineering, National Taiwan University, Taipei, Taiwan, R.O.C .*
[b] *World Premier International Research Center for Materials Nanoarchitectonics, National Institute for Materials Science, Tsukuba, Japan.*
[c] *Japan Science and Technology Agency, Core Research for Evolutionary Science and Technology, Tsukuba, Japan.*
[d] *Research Center for Developmental Biology and Regenerative Medicine, National Taiwan University, Taipei, Taiwan, R.O.C.*
**Shan-hui Hsu (Corresponding author)*
Institute of Polymer Science and Engineering, National Taiwan University, No. 1, Sec. 4 Roosevelt Road, Taipei 10617, Taiwan, R.O.C.; Phone: +886-2-3366-5313; Fax: +886-2-3366-5237; E-mail: shhsu@ntu.edu.tw
**Katsuhiko Ariga (Corresponding author)*
World Premier International (WPI) Research Center for Materials Nanoarchitectonics (MANA), National Institute for Materials Science (NIMS), 1-1 Namiki, Tsukuba 305-0044, Japan; Phone: +81-29-860-4597; Fax: +81-29-860-4832; E-mail: ARIGA.Katsuhiko@nims.go.jp
† Electronic Supplementary Information (ESI) available: Determination of the appropriate timing of adding serum-containing media in the transfection protocol. See DOI: 10.1039/x0xx00000x

transfection reagents into cells because of the negative charge[18,19]. The aminosilane-modified nanowires that tethered the naked plasmid could be used to enhance the plasmid delivery by penetrating through the cell membrane but this method may cause cell damage[20].

Many organic/inorganic hybrid nanoparticles have been widely applied in optical, electronic, and biomedical fields[21]. Poly(ethylene oxide) or DNA in helical structure has been incorporated into silicate or liposome multilamellar membranes to increase the gene delivery efficiency[22,23]. Except nanoparticles or multilamellar membranes, very few organic/inorganic nanostructured hybrids have been reported to increase gene transfection.

In our previous study, silica upright nanosheet network (5 μm in width and 120 μm in height) modified with or without 3-aminopropyltriethoxysliane (APTES) was found to promote the transfection of naked GATA binding protein 4 plasmid DNA into human mesenchymal stem cells (hMSCs) without any transfection reagent, and the possible mechanisms involved were the activation of cell surface receptors and cytoskeleton rearrangement[24]. In spite of these findings, the roles of geometric parameters and chemistry of nanosheets in nanosheet-based gene transfection was not fully understood. In this study, we prepared upright nanosheets with different geometric parameters and chemistry (Figure 1). We examined the gene transfection efficiency to establish the physico-chemical factors that determined the gene delivery on nanosheet network surface. Because we employed neither forward nor reverse transfection in the procedure, we also investigated if the migration behavior of the seeded cells could be used as an indicator for the gene delivery efficiency on nanosheet network surface with different physico-chemical properties.

2. Materials and Methods

2.1. Preparation of various nanosheet networks

For the nanosheet networks with different geometric parameters, a layer of silica (1 μm thick) was sputtered on a 1 cm^2 square silicon, which was then incubated and etched in 0.5 mg/ml sodium borohydride ($NaBH_4$) solution in a 20 ml teflon-lined steel autoclave at 75°C for 3 and 6 h to form the suspended upright nanosheet network. The preparation process of nanosheet networks with different etching times is displayed in Figure 1B. For the nanosheet networks with different chemistry, the silica-coated silicon was immersed in the 0.5 mg/ml $NaBH_4$ solution with 0.3% sodium chloride (NaCl), 3-aminopropyltriethoxysilane (ATPES), polyallylamine hydrochloride (PAH), or water-based biodegradable polyurethane (PU)[25] in the teflon-lined steel autoclave at 75°C for 6 h. After the reaction, the mixture was centrifuged at 600 rpm for 3 min to separate nanosheets and the etching solution. Nanosheets were washed and resuspended in clean water. The nanosheet suspension (600 μl) is then dripped onto 1.5 cm-diameter coverslip glass placed in petri dish, dried for 24 h, and sterilized with ultraviole light for 4 h. The loading amount of nanosheet suspension on coverslip glass was ~0.35 mg/cm^2. The synthesis of water-based biodegradable PU bearing carboxylic group was synthesized as described briefly below. The soft segment of water-based PU was poly(ε-caprolactone) diol (PCL diol), which reacted with isophorone diisocyanate (IPDI, Evonik Degussa GmbH), the first chain extender 2,2-bis(hydroxymethyl) propionic acid (DMPA, Aldrich), and finally the second chain extender triethylamine (TEA, RDH) in water with vigorous stirring to form the PU structure. Therefore, the PU contains urethane (–NHCOO–) and COO^- along the chain and possibly NH_2 at the chain ends[25]. The preparation process of various nanosheet networks is shown in Figure 1C.

The nanosheet suspension was dripped onto coverslip glass and analyzed by scanning electron microscopy (SEM), and the thickness, height, and pore size of the nanosheet networks were quantified by the ImageJ software (National Institutes of Health). The nanosheet suspension (10 μl) was dipped onto copper grids, and characterized for the elements of various nanosheets by the SEM-based energy dispersive X-ray spectrometer (EDX). The surface chemistry was determined by the attenuated total-reflectance Fourier transform infrared (ATR-FTIR) spectroscopy. The surface hydrophilicity was evaluated by measuring the water contact angle (FTA-1000B, First Ten Angstrom Company, USA). The surface zeta potential was determined by the electrophoretic light scattering (Delsa™ Nano C, Beckman Coulter). To confirm that nanosheets could be harvested by the above method, the supernatant was dipped onto 1.5 cm coverslip glass and analyzed by SEM. After harvest of nanosheets, no residual silica nanosheets remained in the etching solution. The observation suggested that the method could separate nanosheets and etching solution completely.

2.2. Culture of mesenchymal stem cells (MSCs) culture and transfection of plasmid DNA

Human umbilical cord derived mesenchymal stem cells (hMSCs, the first passage) were provided by BIONET Corp. (Taiwan). All human subjects and protocols involved were approved by the institutional review board of Chang Gung Memorial Hospital (IRB#92-176). The hMSCs were grown in alpha minimum essential medium (α-MEM, Invitrogen) supplemented with 10% fetal bovine serum (FBS, Gibco), 2.2 g/l sodium bicarbonate (Na_2CO_3, Sigma), and 1% penicillin-streptomycin solution (Invitrogen) at 37°C in a 5% CO_2 incubator. Cells of 5-8 passages were used in the study.

5×10^4 cells/ml hMSCs was added to each well containing different substrates on 1.5 cm planar silica in a 24-well tissue culture plate and incubated in 5% CO_2 at 37°C for 60 h. Cells were cultured with 1 ml of serum-free medium that contained 1 μg naked green fluorescent protein (GFP, pCMV-GFP vector) plasmid for 12 h and the medium was changed to 10% serum-containing medium. After 48 h (at 60 h post seeding), cells were washed with phosphate-buffered saline (PBS), harvested by incubation with 0.25% trypsin, and collected by centrifugation. For the group used to a commercial transfection

reagent (PolyFect, Qiagen, Germany; a dendrimer-based transfection reagent) was employed following the manufacturer's (forward) transfection protocol. hMSCs (5×10^4 cells/ml) were cultured with 1 ml of 10% serum-containing medium on planar silica in the 24-well tissue culture plate. After 12 h, the medium was changed to the 10% serum-containing medium with the GFP plasmid/PolyFect complexes. After 24 h (at 36 h post seeding), the medium was changed to the serum-containing medium without the complexes. After another 48 h (at 84 h post seeding), cells were harvested by trypsin for analysis.

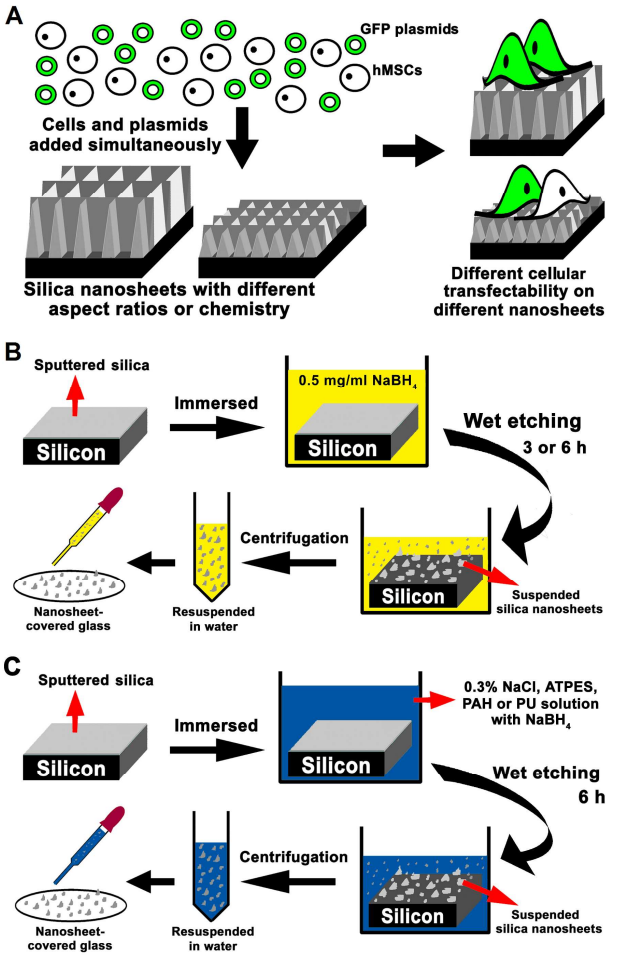

Figure 1. (A) Concurrent transfection of human mesenchymal stem cells (hMSCs) on silica nanosheet networks with different physico-chemical properties. (B) The preparation process of silica upright nanosheet networks with different etching times, which were later deposited on glass. (C) The preparation process of various silica upright nanosheet networks deposited on glass.

2.3. Evaluation of cell survival rate, transfection efficiency, and gene expression

Cells were harvested by 1 ml 0.25% trypsin and collected by centrifugation (1500 rpm, 5 min). The survival rate and transfection efficiency were determined by a flow cytometer (FACS Caliber, BD Biosciences). For the cell survival rate, cell pellets were resuspended in PBS containing 1 µl of propidium iodide and moved into a polystyrene round-bottom tube (12×75 mm style, BD Flacon) for flow cytometer. The survived cells were defined as those without red fluorescence in the overall population. For the transfection efficiency, cell pellets were resuspended in PBS and moved into the polystyrene round-bottom tube for flow cytometer. The transfection efficiency was defined as the percentage of green fluorescence expressing cells in the overall population.

Real-time polymerase chain reaction (RT-PCR) was used to analyze the gene expression of integrin αv and β3 at 12 h. Total RNA was extracted from cells by adding the 1 ml Trizol reagent (Invitrogen). All RNA samples were reverse transcribed individually into cDNA by adding the RevertAid First Strand cDNA Synthesis Kit (MBI Fermentas, St. Leon-Rot, Germany) and amplified by PCR. cDNA reverse-transcribed reaction mixture was made up in 25 µl of 2× SYBR Green PCR master mix and 1 nM of forward and reverse primers (integrin αv sense primer: 5'-GGT CCA TTC TGC ATT GTA TT-3', antisense primer: 5'-ATT TTC TGT CTC ACC CAA TG-3' at 62°C; integrin β3 sense primer: 5'-GTT TTT AGT TGG GAG ATC TGA G-3', antisense primer: 5'-CTA CAT CAG GAG AGA CGT AAC TAT T-3' at 62°C; GAPDH sense primer: 5'-AAC CTG CCA AAT ATG ATG AC-3', antisense primer: 5'-ATA CCA GGA AAT GAG CTT GA-3' at 62°C). The reaction was performed by a Chromo 4 PTC200 Thermal Cycler (MJ Research, USA). The expression levels were analyzed and normalized to GAPDH.

2.4. Analysis of cell migration

To examine the cell mobility, hMSCs cultured on different substrates were recorded by a real-time Cultured Cell Monitoring System (Astec, CCM-Multi, Japan) for 12 h at 10 min intervals. The travelling distance was determined by analysis of the time-lapse images using the ImageJ software. The cell migration rate was calculated as the travelling distance (trajectory) divided by the total recording time. Ten trajectories were analyzed for each sample[26].

2.5. Statistical analysis

The Kayser-Meyer-Olkin (KMO) test and Pearson correlation coefficient were used to evaluate the determining factor of transfection efficiency. These tests assess the level of data explanation from the factors used in the analysis. KMO values at 0.50–1.00 indicate that the data may be appropriate to conduct a factor analysis, while a KMO value lower than 0.50 indicates that the factor cannot satisfactorily describe the variations in the original data. Pearson's correlation coefficient close to -1.00 suggests high correlation. Multiple samples were used in each experiment. The reproducibility was confirmed at least in three independent experiments. Data were expressed as mean standard deviation. Statistical differences were determined by one-way ANOVA analysis. $p < 0.05$ were considered as significant.

3. Results

3.1. Surface characterization of the nanosheet network

The surface chemistry of different nanosheet networks determined by EDX is demonstrated in Table 1. Pristine nanosheet networks produced with different reaction times (6 and 3 h for NS and NS') showed similar atomic ratios of Si and O elements. Once the reaction time was shorter (NS'), the Si content was smaller. When the reaction mixture was added with different chemicals, the surface chemistry of the nanosheet changed with NaCl added, the surface of nanosheet (NS-Cl) contained 5.89% Cl and 4.37% Na. When ATPES was added, the surface of nanosheet (NS-NH_2) comprised 13.62% N and 8.33% C. When the water-based PU was added, the surface chemistry of the nanosheet (NS-PU) displayed the most significant alteration and contained 21.85% N, 16.59% C, and a significantly lower Si (4.3%). When PAH was added in the reaction mixture, the surface of nanosheet (NS-PAH) consisted of 0.8% Cl, 12.98% N, and 3.39% C. The surface functional groups of nanosheets determined by ATR-FTIR are displayed in Figure 2A. The spectra of all nanosheets revealed a peak at ~1000 cm^{-1} associated with Si–O stretching. The spectra of NS-NH_2, NS-PU, and NS-PAH revealed a peak at ~1570 cm^{-1} associated with N–H bending. The spectra of NS-PU and NS-PAH revealed a peak at ~1600 and ~1750 cm^{-1} associated with C=O stretching. The spectra of NS-NH_2, NS-PU, and NS-PAH had peaks at ~2920 cm^{-1} and 2850 cm^{-1} associated with the C–H stretching of $–CH_2$ group. The spectra of NS, NS', and NS-Cl had peaks at ~3400 cm^{-1} associated with O–H stretching. The spectra of NS-NH_2, NS-PU, and NS-PAH had peaks at ~3500 cm^{-1} associated with the N–H or O–H stretching.

Table 1. The chemical composition of various nanosheet networks.

Substrates atomic	Si (%)	Cl (%)	Na (%)	N (%)	O (%)	C (%)
NS	20.56	-	-	-	79.44	-
NS'	14.44	-	-	-	85.56	-
NS-Cl	10.85	5.89	4.37	-	78.89	-
NS-NH_2	15.19	-	-	13.62	62.86	8.33
NS-PU	4.30	-	-	21.85	57.26	16.59
NS-PAH	13.82	0.80	-	12.98	69.02	3.39

Table 2. The geometric parameters of various nanosheet networks.

NS-chemistry	Wall thickness (nm)	Wall height (nm)	Pore diameter (nm)	Surface roughness (nm)	Aspect Ratio*
NS	5±2	120±27	400±128	242±29	24
NS'	400±120	65±20	850±213	985±49	0.16
NS-Cl	400±80	1010±129	1300±550	352±31	2.5
NS-NH_2	25±8	120±49	200±73	3540±482	4.8
NS-PU	17±3	50±6	60±9	1124±339	2.9
NS-PAH	400±102	85±18	170±29	2640±193	0.2

*Aspect ratio= wall height/ wall thickness.

The surface morphology examined by SEM is revealed in Figure 2B (top view) and Figure 2C (angled view). The average geometric parameters calculated by the image analysis are shown in Table 2. Different reaction times led to different geometric factors. The wall thickness, pore size, and surface roughness of NS' were all larger than those of NS. The aspect ratio (wall height/wall thickness) of NS was 24, and it was the highest among all groups. The aspect ratio of NS' was 0.16, and it was the smallest in all groups. Based on these results, we suggested that the addition of different compounds in the reaction mixture could produce nanosheets with different geometric parameters. On the other hand, NS-Cl, NS-PAH, and NS' had largest wall thickness among the groups. NS-Cl had the largest wall height and pore size. NS-NH_2 had the largest surface roughness. The aspect ratios were 4.8, 2.9, 2.5, 0.2 for NS-NH_2, NS-PU, NS-Cl, and NS-PAH, respectively.

The surface zeta potential and contact angle of various nanosheet surfaces are shown in Table 3. The surface zeta potential of NS, NS', and NS-NH2 was -2 to -4 mV, and that of NS-Cl, NS-PU, and NS-PAH was about -7 to -10 mV. The contact angle was approximately in the range of 42-52°.

Table 3. The surface zeta potential and water contact angle of various nanosheet networks.

	Zeta potential (mV)	Contact angle (°)
NS	-3.47±0.38	50.0±2.3
NS'	-3.51±0.22	51.8±3.6
NS-Cl	-7.61±0.31	42.3±1.9
NS-NH_2	-2.55±0.56	46.0±3.7
NS-PU	-9.27±1.72	50.9±2.1
NS-PAH	-9.26±1.87	52.1±2.7

3.2. Cell survival rate and transfection efficiency

The fluorescent images of GFP plasmid-transfected cells on various nanosheet surfaces and those on planar silica with the conventional transfection reagent (PolyFect) are shown in Figure 3A. Cells transfected with GFP plasmid on NS and NS-NH_2 demonstrated the brightest green fluorescence (similar to the PolyFect group), followed by those on NS-Cl and NS-PU. In contrast, cells transfected with GFP plasmid on planar silica (Planar), NS', and NS-PAH displayed only weak fluorescence. The survival rate of hMSCs on Planar and various nanosheet surface exposed to naked plasmid is shown in Figure 3B. All groups had a high survival rate of 80-90%. The group exposed to plasmid/PolyFect complex had a low survival rate of 5%, which was significantly lower than those of nanosheet groups. The transfection efficiency quantified by flow cytometry is shown in Figure 3C. The histograms of transfection efficiency are displayed in Supplementary Figure S1. In brief, cells on NS had the highest transfection efficiency (~70%), which was close to the efficiency of the commercial transfection reagent (~80%). The efficiency on NS-PU, NS-Cl, NS-PAH, NS' was 60%, 60%, 40%, and 25%, respectively, and all of them were significantly greater than that on Planar (~10%).

The possible transfectability determining factor (thickness, height, pore size, surface roughness, zeta potential, and contact angle) of nanosheets were analyzed by the KMO and Pearson correlation test. For KMO test, variables (roughness and zeta potential) had lower levels of communities, and after deletion, the value of KMO was increased to above 0.50. Factor analysis (principal components) was conducted in the control series, and three factors were extracted out (wall thickness, wall height, and pore size). The wall height and wall thickness had the highest values of communities, which may be used to explain the differences in the transfection efficiency of various nanosheets. The Pearson's correlation test furthered confirmed that the wall thickness was the crucial factor for transfection efficiency (with a Pearson's correlation coefficient -0.82).

We therefore hypothesized that combining wall thickness with other parameters may explain the tendency of transfection efficiency. As a matter of fact, plotting the transfection efficiency against ratio of wall height vs. wall thickness (the aspect ratio) of the nanosheet gave rise to Figure 3D. The transfection efficiency fit into a roughly linear curve with the logarithm of aspect ratio.

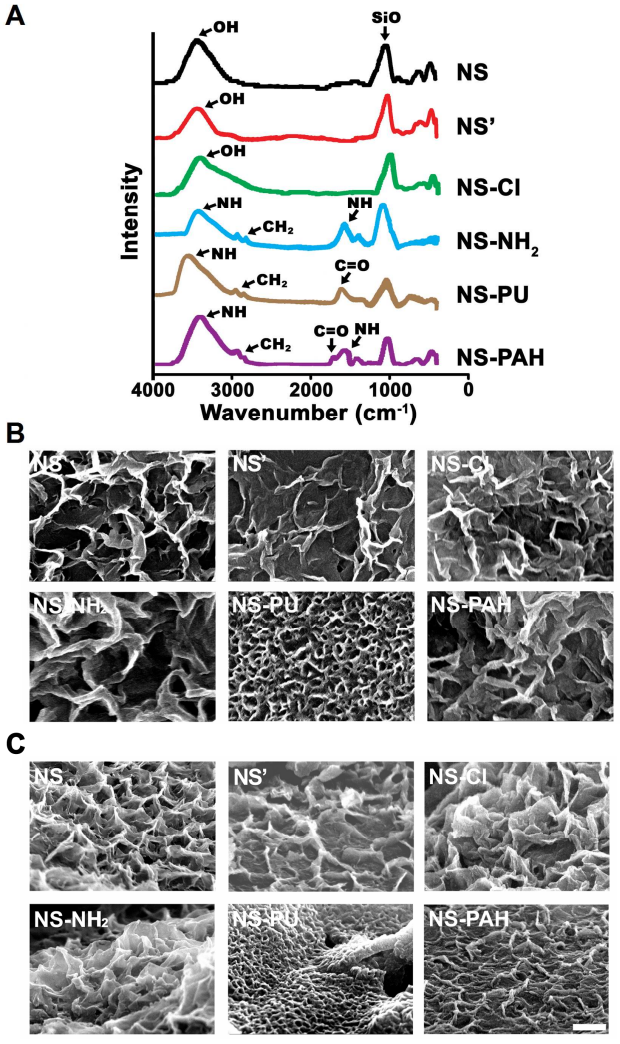

Figure 2. (A) The ATR-FTIR spectroscopy of the pristine nanosheet (NS), pristine nanosheet with shorter reaction time (NS'), and the nanosheets prepared by adding various chemicals in the reaction mixture including with NaCl (NS-Cl), ATPES (NS-NH_2), water-based PU (NS-PU), and PAH (NS-PAH). The SEM images of various nanosheets. (B) Top view and (C) angled view. The scale bar represents 250 nm.

3.3. Cell migration and transfection

The migration rate of hMSCs on various nanosheets during the first twelve hours after seeding was measured and plotted against the logarithm of aspect ratio in Figure 4A. The video recordings for cell migration have been provided in Supplementary data (videos 1–7). It was obviously that cell migration was the slowest (~60 μm/h) on the nanosheet with the smallest aspect ratio (NS') and the greatest (~180 μm/h) on the nanosheet with the largest aspect ratio (NS). Due to corresponding relationship between transfection efficiency and migration rate, we thus suggest that the migration rate could be used for the prediction of transfection efficiency (Figure 4B).

3.4. Cell surface receptor activation

The gene expression levels of integrin αv and β3 in hMSCs on various nanosheets at 12 h are shown in Figure 5. The expression level of integrin αv had a tendency corresponding to the transfection efficiency, and that in NS was significantly greater than those in the other groups. The expression of integrin β3 was significantly different among most nanosheets. The tendency of integrin β3 gene expression was similar to that of the transfection efficiency for hMSCs on various nanosheets. We also combined the gene expression data of integrin αv and integrin β3 of hMSCs on various nanosheets by simple addition, as shown in Figure 5C. The tendency of integrin αvβ3 gene expression was similar to that of the gene expression of integrin β3 on various nanosheets, and had good correlation with the transfectability of hMSCs.

4. Discussion

In substrate-mediated reverse transfection, the chemistry of the substrate can be modified to promote gene transfer. Microcontact printed surfaces containing different functional groups (–CH_3, –COOH, –NH_2, and –OH) preadsorbed with viral vectors were used to transfect HeLa cells. The transfection efficiency was similar among substrates with different chemistries[27]. In contrast, carbon nanotubes modified with –NH_2 groups had better transfection efficiency than those modified with the other functional groups[28]. In our study, the effect of chemistry composition (Cl, Na, N, O, and C) on the transfection of naked plasmid was not obvious. This may be caused by the more remarkable effect of nanosheet geometry on the efficiency of transfection. Besides, a different protocol was employed, that cells and plasmids were simultaneously seeded on the nanosheets without preadsorbed transfection reagent on the surface.

Surface hydrophilicity/hydrophobicity plays a key role in plasmid adsorption during the substrate-mediated reverse transfection. The hydrophobic surface allows more naked plasmid or plasmid/lipid transfection complexes to be

immobilized[29,30] and restricts the cell attachment on the surface[31,32], which enhances the transfection efficiency. Meanwhile, the positively charged surface functionalized by $-NH_2$ and with a proper amount of plasmid adsorbed was favorable for gene delivery[33]. In this study, all nanosheet networks had similar hydrophilicity (contact angle ~42°–50°) but the transfection efficiency was distinct among each other. Therefore, surface hydrophilicity did not account for the different efficiency observed in this study. Moreover, all nanosheet surfaces were negatively charged (-2 to -10 mV), and NS and NS' with similar surface potential but had very distinct gene delivery effect. Thus the surface charge did not explain the difference in transfection efficiency.

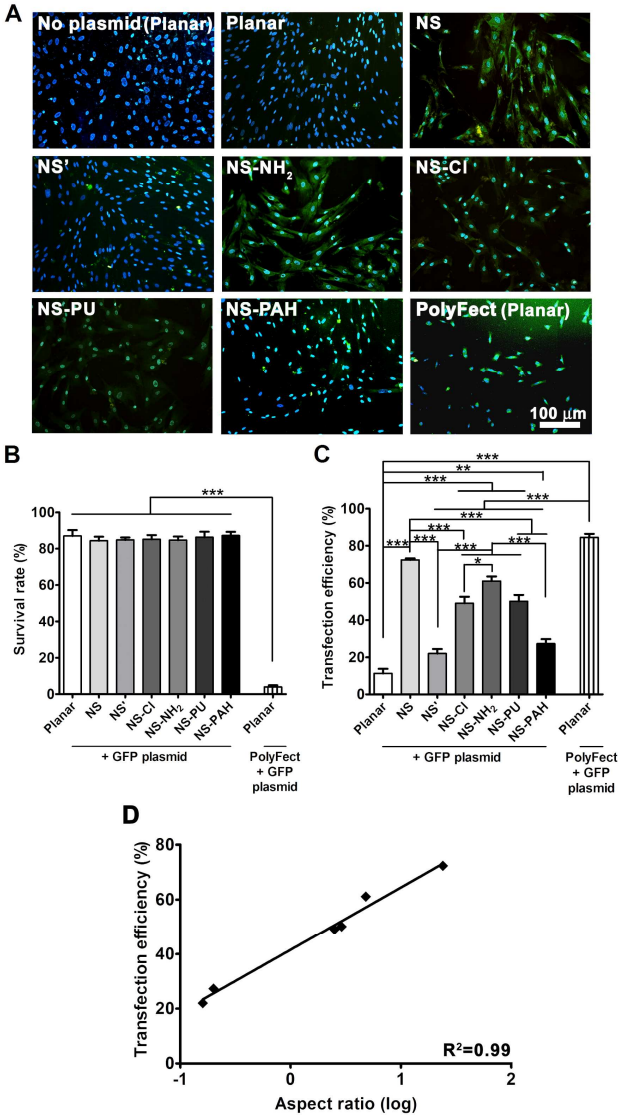

Figure 3. hMSCs transfected with GFP plasmid on NS, NS', NS-Cl, NS-NH_2, NS-PU, and NS-PAH (abbreviation see Figure 2). (A) The fluorescent images, (B) the survival rate, (C) the transfection efficiency, and (D) the relationship between transfection efficiency and logarithm of aspect ratio. All cells were analyzed at 60 h post seeding except for the commercial transfection reagent (TR) group (at 84 h). *, $p< 0.05$; **, $p< 0.01$; ***, $p< 0.001$.

The surface chemistry of nanosheets could be modified by simple addition of various chemicals in etching mixture. However, the geometric parameters were also changed. We suggested that the chemicals (NaCl, ATPES, PAH, and PU) may interfere with the alkaline $NaBH_4$ solution in the etching mixture and further reacted with the surface, leading to the structural change of the hybrid nanosheets. In addition, the surface zeta potential of NS and NS' was similar (~ -3 mV) but the surface morphology of these nanosheets was different. The transfection efficiency of cells on NS and NS' showed a remarkable difference (NS ~70%; NS' ~25%). On the other hand, the surface zeta potential of NS-PAH (~ -9 mV) and NS' (~ -3 mV) was significantly different while the surface morphology of these nanosheets was similar. The transfection efficiency of cells on NS-PAH and NS' showed a significant difference (NS-PAH ~40%; NS' ~25%). Judging from these results, the transfection efficiency was more closely associated with the surface morphology of nanosheets and not the surface zeta potential of nanosheets.

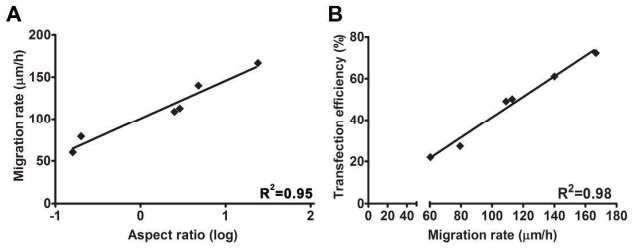

Figure 4. Transfection and cell mobility. (A) The plot to correlate cell migration rate and logarithm of aspect ratio. (B) The plot to correlate cell transfection efficiency and cell migration rate.

In the literature of reverse transfection, substrate topography could affect cell morphology and transfection efficiency. The increased chance of contact between cells and DNA complexes by surface topography may also promote gene delivery[34]. For substrates with micropits, the interspace between the micropits was more critical for transfection than their size[34]. On surface with nanowire arrays, the nanowires of high aspect ratio (with height ~μm and diameter <100 nm) could penetrate cells to facilitate gene delivery[35]. In this study, the surface roughness of the networks and the interspace between the nanosheets were not found to be the main geometric factors to determine the transfection efficiency. The dominant factor was the aspect ratio of the nanosheets. We hypothesized that cells on nanosheets with different aspect ratios may have different motility that may alter their uptake behavior.

The cell adhesion and migration has been reported to affect the formation, maturation, contraction, and disassembly of focal adhesions[32]. The turnover rate of this cycle and the endocytotic activity are both associated with integrin activation[34,36,37]. In this study, the gene expression of integrin αvβ3 as well as the cell migration rate was low on nanosheets with height <90 nm and width >400 nm (low transfection efficiency). When the gene expression of integrin αvβ3 was enhanced, the cell migration rate and transfection efficiency were both enhanced.

The nanosheets examined in our study were a continuous network, and in spite of the large aspect ratio, cell viability remained high. Therefore, nanosheets should have a gene delivery mechanism different from that of nanowires, which involved cell penetration. Based on our cell motility study, nanosheets may activate cell integrin receptor to increase the cell migration rate and uptake behavior. By selecting the appropriate timing of adding serum-containing media (Supplementary Figure S2), cells could better survive, which further enhanced the transfection efficiency.

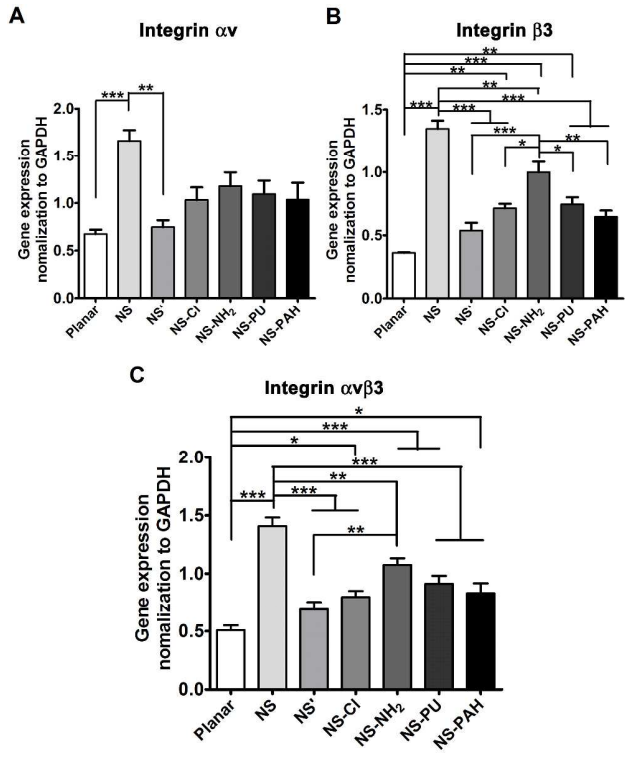

Figure 5. The gene expression levels of cell surface receptors (A) integrin αv, (B) integrin β3, and (C) integrin αvβ3 for cells on NS, NS', NS-Cl, NS-NH_2, NS-PU, and NS-PAH at 12 h post cell seeding. *, p< 0.05; **, p< 0.01; ***, p< 0.001.

In summary, nanosheets with different physico-chemical features could be simply prepared by changing the formula of etching mixture. A network of nanosheets with high aspect ratios could activate integrin and change cell motility (migration rate, uptake behavior, etc). Enhanced migration may also facilitate the cell-plasmid encounter. A positive correlation between cell migration and transfection efficiency was observed, though their exact relationship remained to be identified. The cell migration rate and integrin activation may be used to screen potential nanosheets or nanostructured materials for promoting gene delivery. Moreover, the suspended organic/inorganic hybrid silica nanosheets developed here may be combined with other substrate materials for in situ transfection or temporo-spatial gene delivery applications. All of these require further optimization of the etching process and chemicals to achieve a versatile nanosheet transfection platform.

5. Conclusion

Nanosheet networks of different geometric factors and physico-chemical properties were obtained by changing the reaction mixture and reaction time of the chemical etching process for glass. Suspended nanosheet networks were then deposited on substrates for evaluation of their effect on delivery of naked plasmid DNA to hMSCs. It was demonstrated that surface chemistry, hydrophility, and zeta potential of the nanosheet networks had no significant effect on the transfection efficiency. Among all factors, the aspect ratio of the nanosheets (wall height/width) showed a critical effect on the cell migration rate and gene transfection efficiency on the nanosheets. Plotting the log-log of migration or transfection efficiency against the aspect ratio revealed an almost linear and positive relationship. Therefore, we suggested that the aspect ratio may enhance the transfectability by increasing the cell mobility. The activation of cell surface receptor integrin αvβ3, particularly the integrin β3, accounted for the different mobility of hMSCs on the various nanosheet surfaces. Cell migration rate may thus serve as an index to screen the applicability of the nanosheets on cell transfection. Nanosheets with an aspect ratio of NS demonstrated better transfectability than the other nanosheets while the cytotoxicity remained equally low. Future efforts may focus on further increasing the aspect ratio without physical penetration or damage to the cells and fabricating the organic/inorganic hybrid nanosheets on soft substrates for in situ transfection.

Acknowledgments

This research was supported by the Ministry of Education Taiwan through an international excellence NTU-NIMS collaboration grant (#103R104100) and Ministry of Science and Technology, Taiwan, R.O.C. (MOST103-2321-B-002-100). MSCs of the first passage were supplied by Dr. M. Sieber of rBIONET Taiwan.

References

1 E. Wagner, D. Curiel, and M. Cotton, *Adv. Drug Deliv. Rev.*, 1994, **14**, 113.
2 S. Menuel, S. Fontanay, I. Clarot, R.E. Duval, L. Diez, and A. Marsura, *Bioconjugate Chem.*, 2008, **19**, 2357.
3 I.I. Slowing, J.L. Vivero-Escoto, C.W. Wu, and VS.Y. Lin, *Adv. Drug Deliv. Rev.*, 2008, **60**, 1278.
4 A. Ivorra, J. Villemejane, and L.M. Mir, *Phys. Chem. Chem. Phys.*, 2010, **12**, 10055.
5 W. Kim, J.K. Ng, M.E. Kunitake, B.R. Conklin, and P.D. Yang, *J. Am. Chem. Soc.*, 2007, **129**, 7228.
6 H.H.P. Yiu, S.C. McBain, Z.A.D. Lethbridge, M.R. Lees, and J. Dobson, *J. Biomed. Mater. Res. Part A.*, 2010, **92A**, 386.
7 N.S. Yang, J. Burkholder, B. Roberts, B. Martinell, and D. McCabe, *Proc. Natl. Acad. Sci. USA.*, 1990, **87**, 9567.
8 J.Y. Shiu, C.W. Kuo, W.T. Whang, and P.L. Chen, *Lab on a Chip*, 2010, **10**, 556.

9 H. Wang, T. Kaur, N. Tavakoli, J. Joseph, and S. Wettig, *Phys.Chem. Chem. Phys.*, 2013, **15**, 20510.
10 S.L. Lo, and S. Wang, *Biomaterials*, 2008, **29**, 2408.
11 A.F. Adler and K.W. Leong, *Nano Today*, 2010, **5**, 553.
12 A. Okazaki, J. Jo, and Y. Tabata. *Tissue Eng.* 2007,**13**,245.
13 L. Tang, W. Liu, and G. Liu, *Adv. Mater.*, 2010, **22**, 2652.
14 C.X. He, N. Li, Y.L. Hu, X.M. Zhu, H.J. Li, M. Han, P.H. Miao, Z.J. Hu, G. Wang, W.Q. Liang, Y. Tabata, and J.Q. Gao. *Pharm. Res.*, 2011, **28**, 1577.
15 Q. Ji, T. Yamazaki, N. Hanagata, M.V. Lee, J.P. Hill, and K. Ariga, *Chem. Commun.*, 2012, **48**, 8496.
16 W. Kim, J.K. Ng, M.E. Kunitake, B.R. Conklin, and P.D. Yang, *J. Am. Chem. Soc.*, 2007, **129**, 7228.
17 T. Houchin-Ray, L.A. Swift, J.H. Jang, and L.D. Shea. *Biomaterials*, 2007, **28**, 2603.
18 C.-W. Kuo, J.-J. Lai, K.H. Wei, and P. Chen. *Nanotechnology.* 2008,**19**,025103. doi: 10.1088/0957-4484/19/02/025103.
19 J.-k. Sun, K.-f. Ren, L.-z. Zhu, and J. Ji. *Colloids Surf B Biointerfaces.* 2013,**112**,67.
20 A.K. Shalek, J.T. Robinson, E.S. Karp, J.S. Lee, D.-R. Ahn, M.-H. Yoon, A. Suttona, M. Jorgollic, R.S. Gertnera, T.S. Gujrala, G. MacBeath, E.G. Yang, and H. Park. *Proc. Natl. Acad. Sci. U.S.A.* 2010,**107**,1870.
21 M. Shen and X. Shi. *Nanoscale* 2010,**2**,1596.
22 P. Arand and E. Ruiz-Hitzky. *Chem. Mater.* 1992,**4**,1395.
23 J.O. Rädler, l. Koltover, T. Salditt, and C.R. Safinya. *Science* 1997,**275**,810.
24 N.C. Huang, Q. Ji, K. Ariga, S.h. Hsu, *NPG Asia Mater.* NPG Asia Mater., 2015, **7**, e184. doi:10.1038/am.2015.43.
25 S.h. Hsu, K.C. Hung, Y.Y. Lin, C.H. Su, H.Y. Yeh, U.S. Jeng, C.Y. Lu, S.A. Dai, W.E. Fu, and J.C. Lin, *J. Mater. Chem. B*, 2014, **2**, 5083.
26 C.Y. Huang, C.H. Lin, T.T. Ho, H.C. Chen, M.Y. Chu, W.S. Sun, W.C. Kao, H.S. Hung, S.h. Hsu, *J. Med. Biol. Eng.*, 2013, **33**, 139.
27 K.I. McConnell, J.H. Slater, A. Han, J.L. West, and J. Suh, *Soft Matter*, 2011, **7**, 4993.
28 L. Gao, L. Nie, T. Wang, Y. Qin, Z. Guo, D. Yang, and X. Yan, *Chem. Bio. Chem.*, 2006, **7**, 239.
29 J.B. Delehanty, K.M. Shaffer, and B. Lin, *Biosens Bioelectron*, 2004, **20**, 773.
30 Z. Bengali, A.K. Pannier, T. Segura, B.C. Anderson, J.H. Jang, T.A. Mustoe, and L.D. Shea, *Biotech. Bioeng.*, 2005, **90**, 290.
31 A.K. Pannier, B.C. Anderson, and L.D. Shea, *Acta Biomaterialia*, 2005, **1**, 511.
32 T. Ishizaki, N. Saito, and O. Takai. *Langmuir*, 2010,26,8147.
33 T.H. Nguyen and M. Elimelech, *Biomacromolecules*, 2007, **8**, 24.
34 A.F. Adler, A.T. Speidel, N. Christoforou, K. Kolind, M. Foss, and K.W. Leong, *Biomaterials*, 2011, **32**, 3611.
35 Y. Yang, M.F. Yuen, X. Chen, S. Xu, Y. Tang, and W. Zhang, *Cryst. Eng. Comm.*, 2015, **17**, 2791.
36 J. Carpenter, D. Khang, T.J. Webster, *Nanotechnology*, 2008, **19**, 505103. doi: 10.1088/0957-4484/19/50/505103.
37 E.A. Cavalcanti-Adam, T. Volberg, A. Micoulet, H. Kessler, B. Geiger, and J.P. Spatz, *Biophys. J.*, 2007, **92**, 2964.